Effect of electrode shape on grounding resistances - Part 2

Experimental results and cryospheric monitoring

Tomaskovicova, Sonia; Ingeman-Nielsen, Thomas; Christiansen, Anders V.; Brandt, Inooraq; Dahlin, Torleif; Elberling, Bo

Published in:
Geophysics

Link to article, DOI:
10.1190/GEO2015-0148.1

Publication date:
2016

Document Version
Publisher's PDF, also known as Version of record

GEOPHYSICS, VOL. 81, NO. 1 (JANUARY-FEBRUARY 2016); P. WA169–WA182, 10 FIGS., 4 TABLES.
10.1190/GEO2015-0148.1

Effect of electrode shape on grounding resistances — Part 2: Experimental results and cryospheric monitoring

Soňa Tomaškovičová[1], Thomas Ingeman-Nielsen[1], Anders V. Christiansen[2], Inooraq Brandt[3], Torleif Dahlin[4], and Bo Elberling[5]

ABSTRACT

Although electric resistivity tomography (ERT) is now regarded as a standard tool in permafrost monitoring, high grounding resistances continue to limit the acquisition of time series over complete freeze-thaw cycles. In an attempt to alleviate the grounding resistance problem, we have tested three electrode designs featuring increasing sizes and surface area, in the laboratory and at three different field sites in Greenland. Grounding resistance measurements showed that changing the electrode shape (using plates instead of rods) reduced the grounding resistances at all sites by 28%–69% during unfrozen and frozen ground conditions. Using meshes instead of plates (the same rectangular shape and a larger effective surface area) further improved the grounding resistances by 29%–37% in winter. Replacement of rod electrodes of one entire permanent permafrost monitoring array by meshes resulted in an immediate reduction of the average grounding resistance by 73% from 1.5 to 0.4 kΩ (unfrozen conditions); in addition, the length of the acquisition period during the winter season was markedly prolonged. Grounding resistance time series from the three ERT monitoring stations in Greenland showed that the electrodes were rarely perfectly grounded and that grounding resistances exceeding 1 MΩ may occur in severe cases. We concluded that the temperature, electrode shape, and lithology at the sites have a marked impact on electrode performance. Choosing an optimized electrode design may be the deciding factor for successful data acquisition, and should therefore be considered when planning a long-term monitoring project.

INTRODUCTION

The problem of obtaining good ground contact is well-known to most practicing field geophysicists working with electric resistivity tomography (ERT). Because field transmitters are capable of supplying certain maximum potential difference to drive the current, the electrode grounding resistance may become the limiting factor of successful ERT surveys. However, stepping down to transmission of lower currents negatively affects the signal-to-noise ratio (S/N), with implications for data quality. Several authors have argued that high grounding resistances reduced the quality of measurements (Dabas et al., 2000; Baines et al., 2002; Lundström et al., 2009; Hilbich et al., 2011; Rosset et al., 2013) using it as an indicator of data quality in some cases (Branco et al., 2013).

ERT is particularly suitable for monitoring applications due to its repeatability, relative speed of acquisition, and comparatively ease of data processing. It has become a standard tool in frozen ground research, thanks to its multiple advantages over conventional permafrost monitoring approaches (Scott et al., 1990; Vonder Mühll et al., 2001; Hauck and Vonder Mühll, 2003; Kneisel and Hauck, 2008; Hilbich et al., 2011). It is relatively cost efficient and logistically more convenient than drilling. It has the advantage of providing 2D or 3D spatial variability, as opposed to 1D information inferred from temperature boreholes. It can be operated in auto-

Manuscript received by the Editor 6 March 2015; revised manuscript received 11 September 2015; published online 12 January 2016.
[1]Technical University of Denmark, Department of Civil Engineering, Arctic Technology Centre, Lyngby, Denmark. E-mail: soto@byg.dtu.dk; tin@byg.dtu.dk.
[2]Aarhus University, Department of Geoscience, Aarhus, Denmark. E-mail: anders.vest@geo.au.dk.
[3]Orbicon Greenland, Nuuk, Greenland. E-mail: inbr@orbicon.gl.
[4]Lund University, Engineering Geology, Lund, Sweden. E-mail: torleif.dahlin@tg.lth.se.
[5]University of Copenhagen, Department of Geosciences and Natural Resource Management, Center for Permafrost (CENPERM), Copenhagen, Denmark. E-mail: be@ign.ku.dk.

mated mode, which makes it relevant in remote and inaccessible areas as in the Arctic. Not least, its high sensitivity to phase change between water and ice makes it capable of distinguishing unfrozen water content at subzero temperatures. This implies that time-lapse ERT is capable of detecting ground thawing far before any temperature logs can do so, particularly in warm permafrost near 0°C (Kneisel, 2006; Hilbich et al., 2011). This makes ERT monitoring a valuable tool in assessing the effect of climate warming on the distribution of soil unfrozen water in cold regions.

However, in monitoring applications, the requirements on data quality are high because relative changes of ground resistivity should reflect environmental processes of interest, rather than noise resulting from, among other factors, changing grounding resistances. And yet, extremely high grounding resistances encountered over the freezing periods not only substantially compromise the data quality, but more often than not, they limit the possibility of data acquisition to summer months. Consequently, comparison of temporally sparse ERT data with long-term climate records becomes a challenging task (Hilbich et al., 2011).

In ERT surveying, a few techniques to alleviate the grounding resistance problem have been proposed. Enlarging the surface area of the electrodes in contact with the soil is a common strategy. This can be achieved by inserting the electrodes in the ground as deep as possible (Telford et al., 1990; Zonge et al., 2005), or inserting multiple electrodes in parallel (Reynolds, 1997; Zonge et al., 2005; Kneisel and Hauck, 2008; Rosset et al., 2013). For the purpose of facilitating the current flow from the electrode to the ground, electrodes may be watered with fresh or saline water (Telford et al., 1990; Reynolds, 1997; Zonge et al., 2005) or a conductive gel may be applied (Athanasiou et al., 2007). In arid regions, adding detergents helps to decrease the water surface tension thus improving the wetting of electrode and grain surfaces (Zonge et al., 2005). Measurements on rock may be facilitated by placing water-soaked sponges between the rock and the electrode (Kneisel and Hauck, 2008). Installing the electrodes in clay or mud mixed with water helps to retain moisture over the course of the measurements (Reynolds, 1997; Zonge et al., 2005).

Nonetheless, in automated ERT monitoring, it is mostly too labor intensive, if not impossible, to check and adjust the electrode contact before every measurement launch. Not least, because monitoring projects often span several seasons, the quality of electrode grounding will necessarily vary as result of changing environmental conditions in the ground. Consequently, an array that performs very well in the summer/humid season might become impossible to measure in the winter/dry season. This is particularly the case in cryospheric applications, in which the ERT method typically suffers from high grounding resistances for substantial portions of the year. These limitations require the foreseeable issues to be addressed during the design phase of a monitoring project. As pointed out by LaBrecque and Daily (2008), electrodes are a primary source of errors in resistivity measurement systems. Thus, optimization of electrode design is an essential part of such preparations.

The aim of this study is to improve our understanding of properties and processes affecting the grounding resistance of real electrodes and provide quantitative information on the range of grounding resistances that may occur during ERT monitoring in permafrost areas and other cryospheric applications. We present results of field and laboratory experiments documenting the performance of three electrode types of different size, shape, and surface area under various ground temperature conditions at three field sites of different lithology. We also provide grounding resistance time series measured at three active or past monitoring stations in Greenland, and we attempt to separate the contributions of different processes to the observed grounding resistances.

This is the second of two papers describing our study of electrode grounding resistances. The first paper presents the theoretical basis of the study and the focus-one protocol used for measuring grounding resistances of ERT array electrodes (Ingeman-Nielsen et al., 2016).

Definition of grounding resistance

The grounding resistance R_g (Ω) of an electrode is defined as the potential U (V) at the electrode surface (relative to zero potential at infinite distance) divided by the current I (A) injected by the electrode into the medium in which it is embedded (Sunde, 1949; Wait, 1982; Hördt et al., 2013):

$$R_g = \frac{U}{I}. \tag{1}$$

T. Ingeman-Nielsen and S. Tomaškovičová (personal communication, 2015) and Ingeman-Nielsen et al. (2016) present a framework for calculating the theoretical grounding resistance for rod and plate electrodes. According to their derivations, the grounding resistance of an electrode may be represented as follows:

$$R_g = R_m + R_a, \tag{2}$$

where R_m (Ω) represents the effect of the geometry of the electrode and properties of the embedding medium (the ground resistivity). The second term R_a (Ω) is an additional resistance, which may comprise an interfacial resistance component at the electrode-soil interface and a near-zone anomalous resistivity contribution. The anomalous zone is linked to the disturbance created by the planting and treatment (e.g., watering) of the electrode and possible interaction, such as preferential drying or freezing around the electrode. The additional resistance R_a may be positive or negative depending on the resistivity of the anomalous zone and magnitude of the interfacial component (always positive). If R_a is zero, we consider the electrode *perfectly grounded*.

In practical field applications, measuring the single-electrode grounding resistance is not possible because only differential measurements can be performed. However, the focus-one protocol (Ingeman-Nielsen et al., 2016) provides a convenient way to approximate the grounding resistance of each electrode in a multielectrode array. The focus-one protocol consists of a sequence of measurements, in which the resistance of each electrode is measured in turn against all the remaining electrodes in parallel. It is essentially a "two-electrode" measurement, transmitting current and measuring the potential difference on the same set of electrodes. However, the grounding resistance of one side of the circuit is effectively reduced by connecting many electrodes in parallel, and the measured circuit resistance therefore approximates the single-electrode resistance of the *focus electrode*. Through numerical modeling, Ingeman-Nielsen et al. (2016) show that the measured focus-one resistances are typically within ±7% (or better) of the true single rod grounding resistances for arrays of more than 30 electrodes,

provided that the internal resistance of the instrument is on the order of 10 MΩ or higher.

MATERIALS AND METHODS

With our focus on electrodes as an important source of error, we studied improvements that can be achieved under various ground conditions by using alternative electrode designs. Three types of data are evaluated in this study as follows:

1) Temperature-controlled laboratory experiment: A feasibility study focused on temperature influence on grounding resistances of four electrode configurations.
2) Field comparison of electrode types: Three test sites of different lithology were equipped, each with short arrays of three different electrode designs, and grounding resistances was measured across seasons.
3) Authentic field monitoring applications: Changes of grounding resistance have been monitored at three semipermanent ERT monitoring sites, each equipped with electrodes of a different design. The performance of the arrays is assessed by comparing the grounding resistances and the length of the measurements season. Grounding resistance changes due to the use of two alternative electrode designs are quantified at one of the sites.

Throughout the paper, measurement results are represented as mean ± standard deviation whenever relevant and when multiple measurements or repetitions are available.

Electrodes

The electrode designs chosen for testing were short-rod electrodes, square-plate electrodes, and square-mesh electrodes (see Figure 1). The electrodes were chosen to allow a study of the effect of shape and size (comparing rods and plates) and the effect of increasing surface area of similarly shaped electrodes (comparing plates and meshes). All electrodes were made of stainless steel to reduce the influence of material properties, and their dimensions and properties are listed in Table 1. The mesh electrodes were composed of four layers of stainless steel wire mesh with a thread diameter of 1 mm and a mesh density of 3.86 per centimeter. All electrodes were connected to the measurement instrumentation by copper wire attached to the electrodes with nuts and bolts, as visible in detail in Figure 1c.

Temperature-controlled laboratory experiment

In an attempt to separate temperature effects (ground freezing/thawing) on grounding resistances from other environmental factors, we conducted a laboratory experiment in a temperature-controlled climate chamber, measuring the resistance of individual electrodes in small buckets at different temperatures.

Thirty-two plastic buckets (diameter: 26.9 cm [top]/23 cm [bottom] and height 23.6 cm) were lined with aluminum foil and filled with a silty clay material from Kangerlussuaq, west Greenland. The silty clay material was thoroughly homogenized in a large industrial mixer, whereas distilled water was added to make up for moisture loss during storage. Approximately 8 kg of the silty clay was placed in each bucket. The final gravimetric water content was measured by oven drying of three samples from each bucket. The gravimetric water content in all the buckets varied in a range between 37.6% and 43.4% with a mean and standard deviation of 40.1 ± 1.5%.

The buckets were arranged in four rows and eight columns. The first row contained eight horizontally oriented rod electrodes, the second row contained vertically oriented plate electrodes, the third

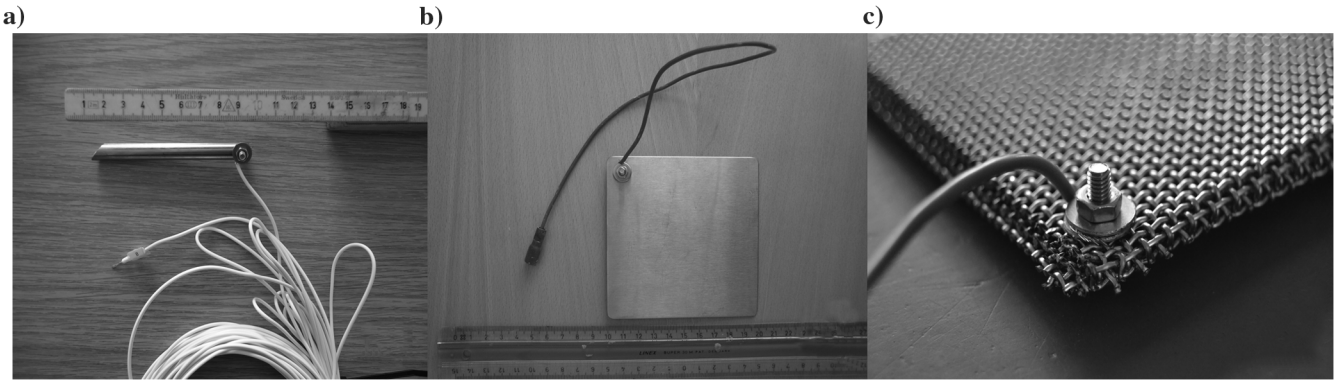

Figure 1. Electrode designs tested: (a) rod electrode with attached copper cable, (b) plate electrode, and (c) mesh electrode.

Table 1. Properties of the physical electrodes used in field and laboratory testing.

	Rods	Plates	Meshes
Dimensions	$\phi = 1.0$ cm, $L = 8.0$ cm	$10 \times 10 \times 0.1$ cm ($h \times w \times t$)	$10 \times 10 \times 0.6$ cm ($h \times w \times t$)
Estimated effective surface area	27 cm^2	204 cm^2	985 cm^2
Material	Stainless steel	Stainless steel	Stainless steel

row contained horizontally oriented plate electrodes (Figure 2b), and the fourth row contained vertically placed mesh electrodes. The total height of the clay mixture in each bucket was approximately 15 cm. The vertically placed electrodes were covered by 1 cm, and the horizontally placed ones by 5 cm of clay mixture. To take full advantage of the large effective surface area of the mesh electrodes, the mesh openings were filled with the clay mixture before installation.

Insulated copper wires were attached to each electrode with a nut and bolt, and, similarly, wires were attached to the aluminum foil lining of each bucket. During measurements, the wires from a specific electrode and the aluminum-foil lining of the corresponding bucket were connected to the two terminals of the instrument and used for simultaneous current injection and potential measurement. The lining thus functioned as a very large electrode ensuring that the resistance between the two terminals of the instrument was primarily controlled by the properties of the single rod, plate, or mesh electrode installed in the bucket.

A thermistor was placed in the first bucket of each row to measure the temperature of the soil in the bucket. Finally, a lid was placed on each bucket to reduce moisture loss during the experiment.

The buckets were placed on Styrofoam pads, and isolating material was placed around and between the buckets to encourage a one-sided freezing pattern (Figure 2a). The buckets were placed in a climate chamber in which they rested for 24 h before the testing began. In the following days, three sets of measurements were performed at -1.4 ± 0.3°C, -14.3 ± 0.6°C, and finally at 19.9 ± 0.8°C. A resting period of 24 h after each temperature step allowed the temperature within the buckets to stabilize.

We measured the total circuit resistance of each bucket using an ABEM Terrameter SAS 1000, using a current of 1 mA with a 100% duty cycle square waveform and a period of 1 s. Voltage measurements were acquired over the last 0.3 s of each on time, and results of five periods were averaged. The results of this experiment are reported in the "Results: Temperature-controlled laboratory experiment" subsection.

Description of selected field sites

Three sites in central west Greenland were selected for testing of the electrode designs under realistic field conditions. The sites were selected based on the availability of current or past ERT time-lapse monitoring data.

The Qeqertarsuaq site (69° 15′N, 53° 30′W, 30 m above sea level) is located at Østerlien, near the Arctic Station on Qeqertarsuaq/Disko Island in a tundra landscape/environment. Disko Island is located in the transitional zone between the Low and High Arctic. According to meteorologic data of nearby Arctic Station (Hansen et al., 2006), mean air temperatures of the warmest (July) and the coldest (February to March) months are 7.1°C and −16.0°C, respectively. The mean annual soil temperature at 5 cm depth is −1.9°C. Accordingly, the site is located in the discontinuous permafrost zone, and no permafrost was observed from ground temperature measurements at the actual site location to a depth of 3.5 m. The study site is situated in a bedrock valley filled with loose Holocene sands and gravels with a typical topsoil thickness of 5–10 cm. The crystalline basement (granite) and Tertiary breccia plateau basalts are visible in outcrops around the area. Among other important environmental parameters, air and soil temperature and soil moisture content are recorded at the site.

The Ilulissat site (69° 14′N, 51° 3′W, 33 m above sea level) is situated near the airport of the town of Ilulissat on the mainland in the inner part of the Disko Bay. The site is located in the continuous permafrost zone (Brown et al., 1998), and the mean annual air temperature (MAAT) is −5.1°C (2003–2012, data from Cappelen, 2013, Danish Meteorological Institute, tech. rept. 3-11). The active layer thickness at the site is approximately 80 cm, below which ice-rich permafrost is found. The sediment cover consists of postglacial silt and clay marine deposits. These deposits are fully leached in the upper part, with the residual salinity increasing with depth, causing the deeper parts of the soil profile to be technically unfrozen due to the freezing point depression. Gneiss bedrock is encountered at the site at a 7 m depth. Unfrozen soil water content in the active layer in the thawed period ranges from 60% to 70% at nearly full saturation.

The Sisimiut site (66° 56′N, 53° 36′W, approximately 48 m above sea level) is located in a valley east of the town of Sisimiut. The area is affected by discontinuous permafrost (Brown et al., 1998) with an MAAT of −1.1°C (2003–2012, data from Cappelen, 2013, Danish Meteorological Institute, tech. rept. 3-11). The top part of the sedimentary sequence is dominated by sandy freshwater deposits underlain by postglacial marine clayey silt deposits (Ingeman-Nielsen, 2005). The topsoil thickness is typically less than 5 cm. The area is shaded by a large mountain ridge to the south, causing the site location to be expectedly colder than the meteorologic data from the town station indicates (located near the coast a few kilometers from the site). The active-layer thickness is approximately 1.0 m at the site, which is well-drained and slightly elevated, causing little snow to accumulate in winter. However, the active-layer thickness varies in the immediate surroundings, depending on peat and topsoil thicknesses, lithology, and drainage conditions, which all show considerable variability.

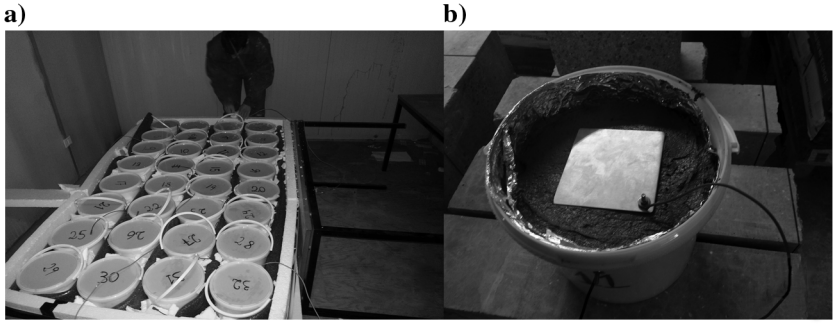

Figure 2. Temperature-controlled laboratory experiment setup: (a) arrangement of 32 buckets with test electrodes in a cold chamber and (b) placement of the horizontal plate electrode in an aluminum-foil-lined plastic bucket filled with the clay mixture and covered by 5 cm of clay material.

Electrode field experiment setup and measurement procedure

Experimental test sites were established at each of the three monitoring field sites for testing the three different electrode designs under different soil conditions. At each site, three arrays of 10 mesh electrodes, 10 plate electrodes, and 10 rod electrodes were installed. Mesh and plate electrodes were installed vertically in the ground so that the plane defined by the electrode is perpendicular to an imaginary line connecting the centers of all electrodes of that type. If the nature of the soil allowed, the mesh openings of the mesh electrodes were filled with local material (Figure 3c). Rod electrodes were installed with the rod length axis in the horizontal direction and perpendicular to an imaginary line connecting the rod electrodes. All electrodes of the same kind were spaced 30 cm apart; the arrays of respective electrode types were likewise spaced 30 cm apart. If the center of the first mesh electrode was at (0.0, 0.0) m, the center of the last rod electrode thus was at (2.70, 0.60) m (Figure 3a).

The electrodes were buried at a depth of 5–10 cm, depending on the conditions of the field site, to protect them from damage and removal by animals, and for ensuring installation in actual soil (and not debris and mosses at the surface).

Grounding resistances of the electrodes at all three sites were measured in summer, fall, and winter 2013/2014. The individual electrode grounding resistances were measured using the focus-one protocol for each of the three arrays in turn, using an ABEM Terrameter SAS 1000 or an ABEM Terrameter LS, depending on availability. The current during grounding resistance measurements was fixed at 1 mA, using a 100% duty cycle square waveform with a period of 1 s. Voltage measurements were acquired over the last 0.3 s of each on time, and the results of five periods were averaged. The results of these experiments are reported in the "Results: Electrode field experiment" subsection.

Long-term monitoring arrays

At the Qeqertarsuaq site, the ERT monitoring station was set up in July 2013 and scheduled to collect several resistivity profiles a day throughout the freezing season until the end of February 2014 (Doetsch et al., 2015). The monitoring was carried out on two parallel lines (2 m apart) with 64 electrodes each (although Doetsch et al. [2015] report data from only one of the two lines), electrode spacing 0.5 m for the 42 electrodes at the center of each line, and 2 m spacing for the electrodes at the ends of the layouts. The arrays were installed using stainless steel plate electrodes with dimensions of $10 \times 10 \times 0.6$ cm, buried at a 5–10-cm depth. The site was instrumented with an ABEM Terrameter LS and an external switchbox ABEM ES10-64 and connected to the Internet for remote control, data download, and monitoring of system conditions. The automated data acquisition program was initially set to collect 7359 resistivity measurements per day using all 128 electrodes, but the sequence had to be reduced after ground freezing commenced due to problems of increasing grounding resistance. After the reduction, 1464 measurements were collected per day using only one array, and 0.5 m spaced electrodes. The grounding resistances of all electrodes were measured daily using the focus-one protocol throughout the entire acquisition period.

The monitoring station at Ilulissat was set up in August 2012 and comprised an array of 64 electrodes with uniform spacing of 0.5 m. The station was equipped with an ABEM Terrameter SAS 1000 and an external switchbox ABEM ES10-64, and it was scheduled to measure 1625 resistivity measurements once a day. Initially, the station was operating in time-lapse mode with no possibility of remote control. Due to instrument limitations, repeated electrode grounding measurements could not be scheduled in the time-lapse mode, and thus they were only collected upon site visits. In February 2014, the station was upgraded for remote control and data transmission. This upgrade also allowed daily measurements of electrode grounding

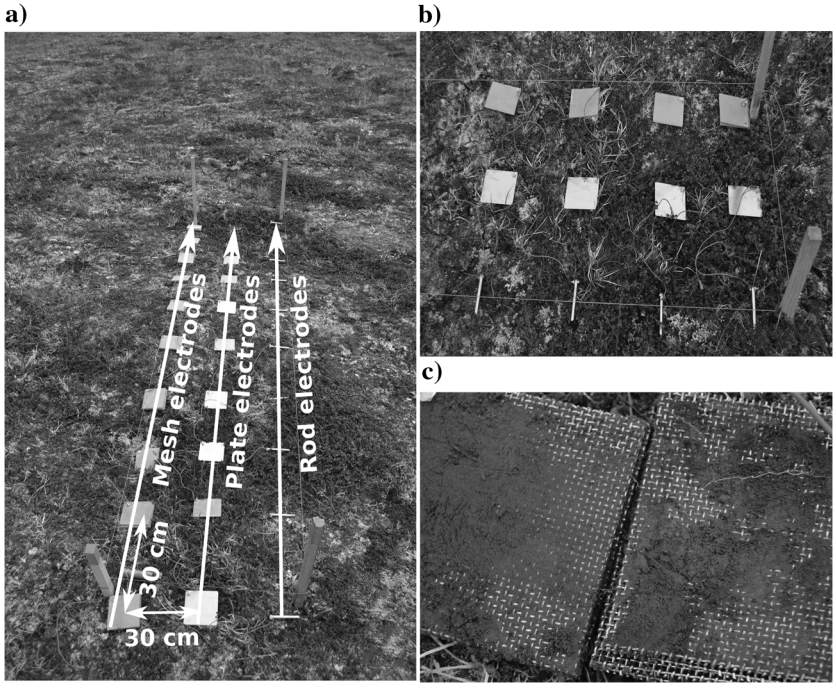

Figure 3. (a) Layout of the electrode field test site indicating electrodes placement and spacing between electrodes, (b) detail of the electrode arrangement, and (c) mesh openings were filled with local soil to take advantage of the increased surface area.

resistance using the focus-one protocol. Initially, the station was equipped with stainless steel rod electrodes (length 8 cm and diameter 1 cm). However, after encountering contact problems relating to ground freezing in late December 2012, all electrodes were replaced by mesh electrodes with dimensions $10 \times 10 \times 0.6$ cm in August 2013.

At Sisimiut, the monitoring array was installed in July 2010. It comprised an array of 64 electrodes with uniform spacing of 0.5 m. The electrodes were stainless steel rods (length 10 cm and diameter 1 cm) buried at a depth of 5–10 cm, oriented horizontally, and with the long axis perpendicular to the array. The array was measured using an ABEM Terrameter LS (using the internal 64-electrode switchbox), but because the site had no power-line access, measurements were initiated manually at irregular intervals. Over the fall, the array was measured several times per week, whereas in the winter months of 2010/2011, intervals increased to monthly or bimonthly. Typically protocols of approximately 2000 resistivity measurements were used, but in winter, electrodes were affected by high grounding resistances, significantly reducing the number of measurements (unique four-electrode combinations) that could actually be collected. Electrode grounding resistance measurements were collected using the focus-one protocol before each data acquisition, and they are thus available at the same temporal intervals. The results of these monitoring experiments are reported in the "Results: Monitoring applications" subsection.

RESULTS

Temperature-controlled laboratory experiment

The results of the temperature-controlled laboratory experiments are summarized in Table 2 and visualized with box plots in Figure 4. A pronounced increase in the total circuit resistance is observed due to freezing. The change is approximately two orders of magnitude between the warmest (+19.9°C) and coldest (−14.3°C) temperatures. At all three temperatures tested, the choice of electrode seems to affect the total circuit resistance, with rods performing the worst (largest resistances and variance); followed by horizontal plates; vertical plates; and finally meshes, which exhibit the lowest measured circuit resistances among all electrodes. The mesh electrodes also exhibit the lowest variation in circuit resistance at all temperatures, although the variation is larger at subzero temperatures for all types of electrodes.

To test the significance of these observations, we have applied a two-way analysis of variance (ANOVA) to the data (Montgomery, 1997), treating the electrode types and temperatures as categorical factors and assuming a log-normal distribution of resistances. We conclude that the main effects of the electrode type and temperature are statistically significant and that there is also significant interaction between electrode type and temperature. On this basis, we applied Tukey's range test (Tukey, 1949) to compare the means of the effects of electrode type at each temperature. The means are all

Table 2. Averages (arithmetic) and standard deviations of total circuit resistances measured in the laboratory experiment at three different temperatures on three electrode types (four configurations), along with the number of involved measurements. Here, *N* refers to the number of electrodes (buckets) that were included in averaging; H and V signify a horizontal and vertical orientation of the plates, respectively.

Temperature	Rods (kΩ)		Plates H (kΩ)		Plates V (kΩ)		Meshes (kΩ)	
$+19.9 \pm 0.8$°C	0.3 ± 0.04	$(N = 6)$	0.1 ± 0.01	$(N = 5)$	0.1 ± 0.01	$(N = 6)$	0.1 ± 0.01	$(N = 6)$
-1.4 ± 0.3°C	1.8 ± 0.7	$(N = 8)$	1.2 ± 0.2	$(N = 7)$	1.0 ± 0.4	$(N = 8)$	0.6 ± 0.1	$(N = 8)$
-14.3 ± 0.6°C	23.3 ± 7.5	$(N = 8)$	19.6 ± 4.9	$(N = 8)$	14.7 ± 6.4	$(N = 8)$	9.0 ± 2.1	$(N = 8)$

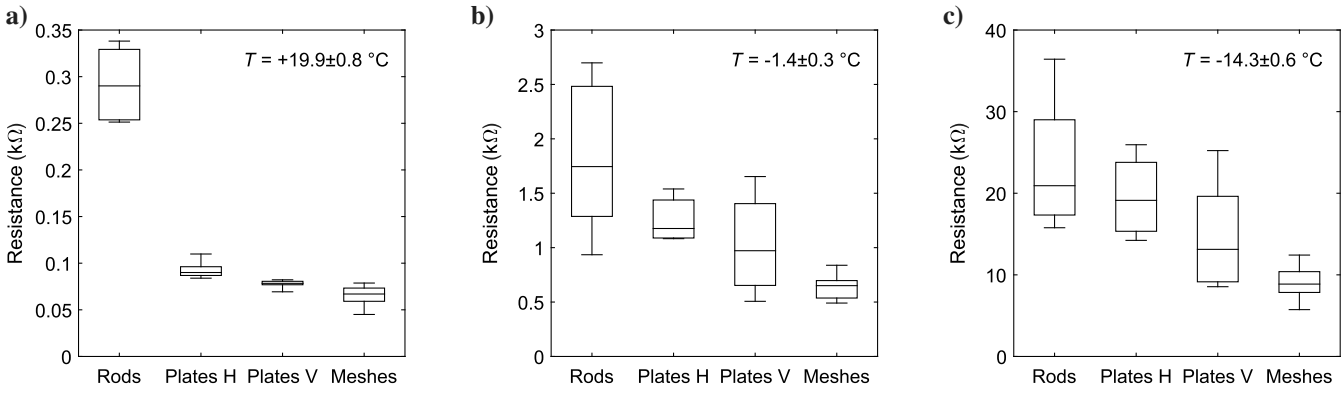

Figure 4. Box plots showing the variation in measured focus-one resistance for eight electrodes of each kind/orientation. The height of the box represents the interquartile range of the data set, and it extends from the 25th to 75th percentile. The horizontal bar within the box indicates the median value, and the whiskers extend to the maximum and minimum (average) values recorded for the given electrode type. The H and V signify the horizontal and vertical orientation of the plates, respectively. The actual number of electrodes involved in plotting each box plot is specified in Table 2.

significantly different ($p < 0.01$) except the means of the rods and horizontal plates at the coldest temperature, which did not differ significantly ($p > 0.05$).

It should be noted that due to the different shapes and orientations of the electrodes and the limited size of the buckets, it cannot be ruled out that some of the variation in total circuit resistance could be explained by variations in current flow patterns that would not be observed in a field setup. For the same reason, the values obtained in the experiment are not applicable to field situations. Nevertheless, because the vertically oriented plates and the meshes have similar shapes and orientations in the buckets, the observed difference between these electrode types can be considered conclusive, and similar effects would be expected in the field.

Ice buildup around electrodes

At the lowest temperature −14.9°C, we selected two buckets of each electrode configuration and cut them in half to visually inspect the effect of freezing processes in the soil around the electrodes. During ground freezing, pore water may migrate to the freezing front and create ice lenses (e.g., Arenson et al., 2005) that could affect the performance of the electrodes. The images in Figure 5 show preferential ice buildup around the metal electrodes, most severely around the plate electrodes. Especially, the horizontally oriented plate shown in Figure 5b has accommodated the growth of a horizontal ice lens immediately above the electrode, effectively isolating one side of it from the surrounding soil, and arguably contributing to the poor performance of horizontal plates. We did not observe significant ice buildup around the rod and mesh electrodes. The size of the rods and construction of the meshes possibly result in a smaller perturbation of the temperature field as compared with the solid plates, which could explain the lower affinity for ice buildup.

Electrode field experiment

Data collected at the three field test sites are summarized in Table 3 and visualized in box plots in Figure 6. The standard deviation of repeated measurements at a particular electrode was typically less than 3% of the measured resistance value. These averaged resistances were used to plot and calculate the general statistics.

The data agree with the findings of the laboratory experiment, with rods generally showing higher focus-one resistances than plates, which in turn have higher focus-one resistances than mesh electrodes. We also observe a strong temperature effect (effect of ground freezing), with focus-one resistances increasing by two to three orders of magnitude between unfrozen and coldest (frozen) conditions. Notably, on the site visit at Sisimiut in March 2014, grounding resistances of all electrodes of the rod type had grown so high that the instrument was incapable of measuring the focus-one resistances (indicating individual grounding resistances larger than approximately 1.2 MΩ). Similarly, approximately half of the mesh and plate electrodes could not be measured.

Because with the laboratory results, a two-way ANOVA has been applied to the data from each of the three sites, treating electrode types and temperatures as categorical factors and assuming a log-normal distribution of measured focus-one resistances. For all sites, we conclude that the main effects of electrode type and temperature are statistically significant and that there is also significant interaction between electrode type and temperature. On this basis, we applied Tukey's range test to compare the means of the effects of electrode type, and we conclude that the rods have significantly higher ($p < 0.01$) grounding resistance than plates and meshes at all temperatures and all sites (except Sisimiut in March, where no statistics could be calculated).

In Ilulissat and Qeqertarsuaq, the focus-one resistance of meshes is significantly lower ($p < 0.01$) than that of the plates at subzero temperatures in October 2013 and February 2014. However, the difference is not significant ($p > 0.05$) in the summer, when the ground is thawed. At the Sisimiut site, the meshes and plates cannot be considered significantly different ($p > 0.05$) at any time of year.

Based on these results, we conclude that mesh electrodes are a significant improvement over other electrode types at two out of three test sites (Ilulissat and Qeqertarsuaq). The rods show the high-

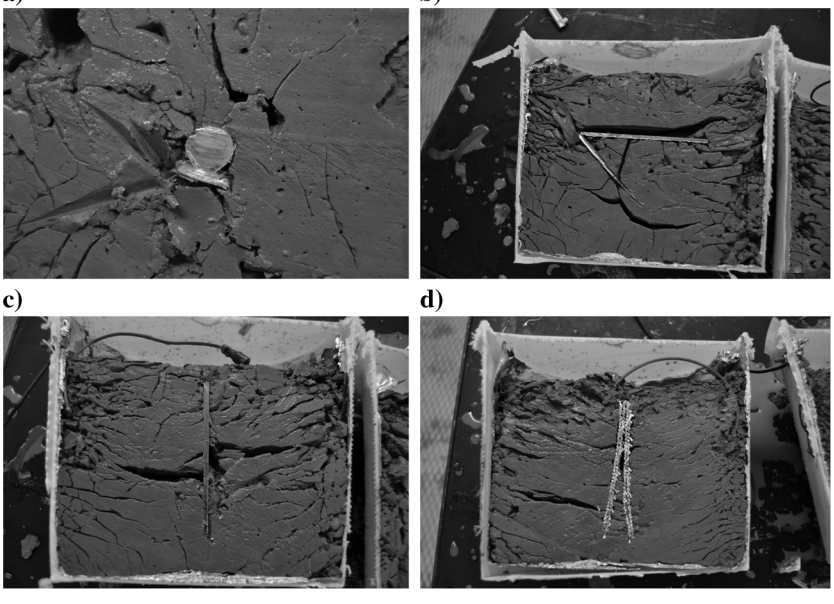

Figure 5. Photos of buckets with the four electrode configurations tested: (a) horizontally oriented rods, (b) horizontally oriented plates, (c) vertically oriented plates, and (d) vertically oriented meshes. Buckets were cut open while deep frozen at −14.9°C, to observe the effect of ice buildup around the electrodes. The ice has melted during the cutting, but the cryo patterns have been preserved as voids, observable as black areas in the images. The preferential freezing patterns particularly affect the plate electrodes of both configurations and are suspected to be a main factor in their decreased electrode performance at subzero temperatures.

est grounding resistances at all sites and all times of year. This includes Sisimiut in March, where the number of electrodes that could not be measured is used as an indication of electrode performance. The performance differences seem related to site conditions, where Sisimiut is seen to exhibit markedly higher grounding resistances, even in summer, compared with the other sites. This difference is believed to be related to lithology and drainage conditions at the site, but possibly also to the ground temperature regime and permafrost conditions, which would affect the overall half-space resistivity, and thus the embedding medium contribution to the grounding resistance.

Monitoring applications

At the ERT monitoring site in Ilulissat, we first experienced the severe effects of extremely high grounding resistances following the onset of the ground freezing in October 2012. Although no direct measurements of grounding resistances are available from that period, records show that transmitted current was decreasing and the number of daily resistivity measurements that could be collected was decreasing, suggesting increasing grounding resistances. By the end of November, approximately a month after the ground freezing had begun, the grounding resistances reached magnitudes that made it impossible for the SAS 1000 instrument to transmit even the lowest current (1 mA). By the end of December 2012, the ground freezing progressed to a point at which 98% of the daily resistivity measurements could not be measured (see Figure 8).

The success of the laboratory experiments prompted us to replace the rod electrodes by mesh electrodes during the site visit in August 2013. The grounding resistances of rods were recorded on the last day these were in the ground. On the following day (day 1), the rod electrodes were replaced by mesh electrodes. The grounding resistances of the new mesh electrodes were measured on the day of replacement and for 10 consecutive days. Because there was no rainfall event or distinctive temperature change over this period, we consider the environmental conditions for both electrode types to be comparable. We observed immediate and significant (t-test, $p < 0.01$) improvement of grounding resistance following the electrode replacement because the average grounding resistance dropped from 1.5 ± 0.9 kΩ for rods to 0.4 ± 0.1 kΩ for meshes; see Figure 7a. Comparison of the grounding resistances of the two types of electrodes on 29 April 2013 (rods) and 29 April 2014 (meshes) also reveals a significant (t-test, $p < 0.01$) reduction in grounding resistances of the monitoring array, with an average grounding resistance of 25.2 ± 11.4 kΩ for the 64 mesh electrodes (2014), as opposed to 64.1 ± 32.1 kΩ for the rod electrodes (2013), under similar ground temperature conditions (Figure 7b).

Figure 8b shows the number of collected resistivity measurements per day over the entire period that the Ilulissat station has been operational. Although the array was equipped with rod electrodes (the dark gray shading), the onset of freezing was followed by a substantial decrease in the number of daily resistivity measurements collected. When the ground temperature reached approximately −15°C in the beginning of January, the number of measurements had dropped to only 31 records per day. Although the exact grounding resistance values of the monitoring array electrodes from that period are unavailable, the corresponding grounding resistances measured for the short test arrays (see Figure 6 and Table 3) indicate a plausible range of 0.l–0.2 MΩ.

Performance of the array dramatically improved following the electrode replacement in August 2013. Since then, we were able to collect nearly complete data sets throughout the entire winter season, with at most 52 resistivity measurements skipped on a single day. Still, operation of the station was seriously affected by instrument software problems with large data gaps as a result. The station upgrade for remote control and data download completed in February 2014 has significantly reduced station downtime. As an added benefit, we have been able to measure the focus-one resistance of all electrodes at the site on a daily basis.

Table 3. Averages (arithmetic) and standard deviations of grounding resistances measured across seasons at three field experimental sites, along with the number of involved measurements. The *n* specifies the number of measurement repeats collected for each focus electrode, whereas *N* refers to the number of electrodes of the given type that could actually be measured; "n.m." (not measured) indicates that no electrodes of the given type could be measured due to high grounding resistances.

Time	Location	Rods (kΩ)		Plates (kΩ)		Meshes (kΩ)		Soil temperature at 10 cm
July/August 2013 ($n = 5$)	Qeqertarsuaq	1.8 ± 0.2	($N = 10$)	1.3 ± 0.2	($N = 10$)	1.2 ± 0.2	($N = 10$)	+8.8°C
	Ilulissat	1.2 ± 0.1	($N = 10$)	0.6 ± 0.1	($N = 10$)	0.6 ± 0.1	($N = 10$)	+9.5°C[6]
	Sisimiut	16.6 ± 4.9	($N = 10$)	9.2 ± 2.4	($N = 10$)	6.9 ± 1.3	($N = 10$)	+3.8°C[7]
October 2013 ($n = 5$)	Qeqertarsuaq	15.8 ± 3.1	($N = 10$)	4.9 ± 1.1	($N = 10$)	3.3 ± 1.0	($N = 10$)	−0.3°C
	Ilulissat	31.0 ± 4.4	($N = 10$)	17.7 ± 3.0	($N = 10$)	12.6 ± 2.6	($N = 10$)	−2.6°C
	Sisimiut	285.6 ± 56.5	($N = 7$)	162.6 ± 42.7	($N = 10$)	177.1 ± 44.4	($N = 9$)	−0.3°C
February/ March 2014 ($n = 5$)	Qeqertarsuaq	1055.3 ± 65.3	($N = 4$)	555.4 ± 121.9	($N = 10$)	351.2 ± 48.8	($N = 10$)	−10.1°C
	Ilulissat	144.5 ± 26.4	($N = 10$)	97.7 ± 17.1	($N = 10$)	65.8 ± 11.4	($N = 10$)	−10.4°C
	Sisimiut	n.m.	($N = 0$)	1055.5 ± 111.3	($N = 4$)	1171.4 ± 132.6	($N = 5$)	−9.9°C)[8]

[6]Temperature obtained three days after electrode measurements due to data logger malfunction.
[7]Average temperature of the month of August due to data logger malfunction in the days around electrode measurement.
[8]Average ground surface temperature on the day of electrode measurements.

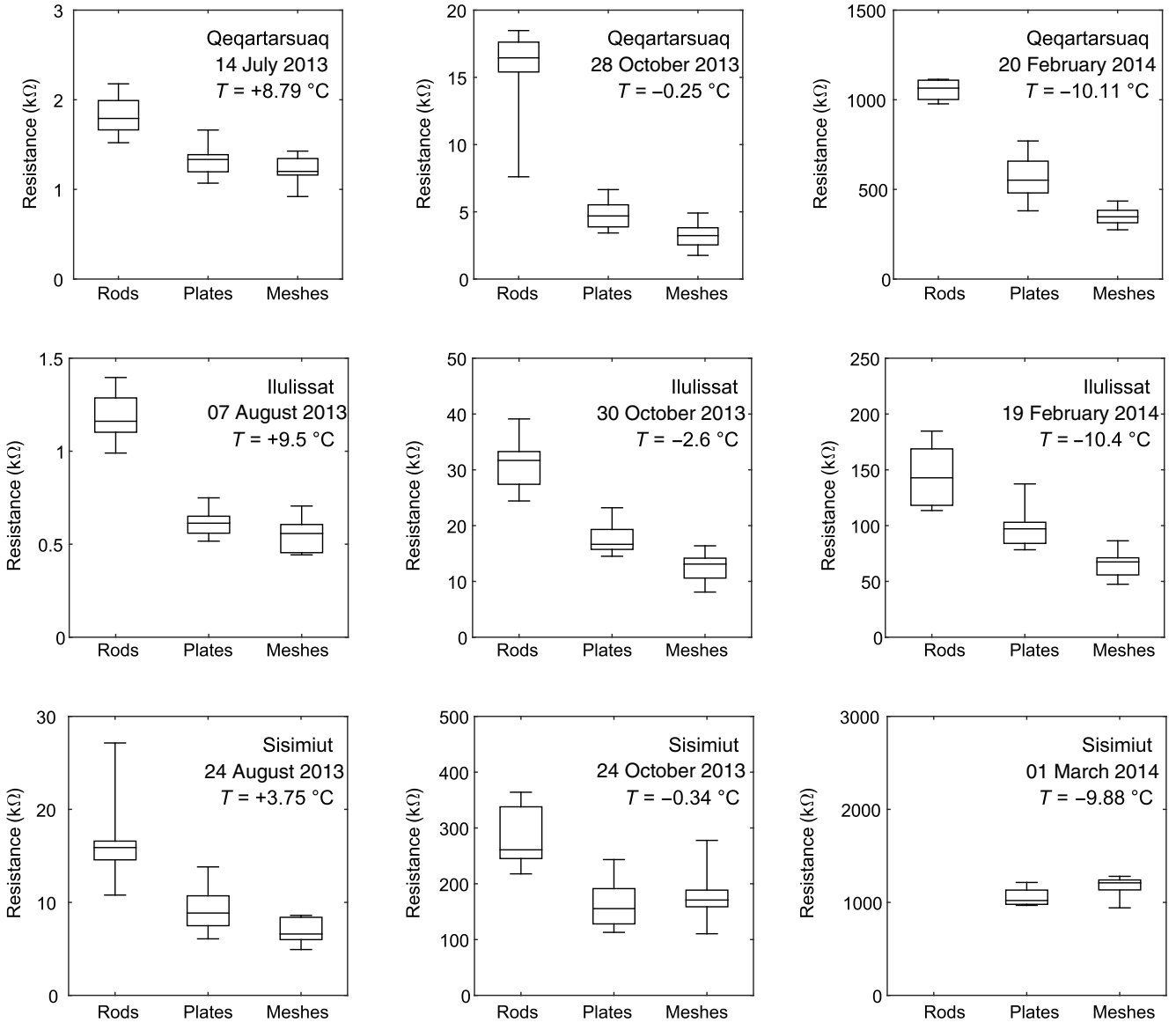

Figure 6. Box plots showing the variation in measured focus-one resistance for the three type of electrodes at the three field test sites. The height of the box portion represents the interquartile range, and the horizontal bar represents the median value. The whiskers extend to the maximum and minimum (average) values recorded for the given electrode type. The actual number of measurements involved in each box plot may be obtained from Table 3.

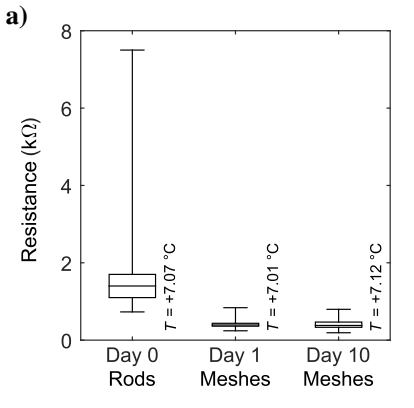

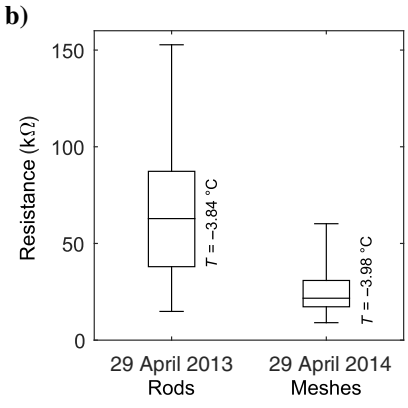

Figure 7. Comparison of electrode focus-one resistances for rod and mesh electrodes following the replacement at the Ilulissat monitoring station: (a) immediate reduction of grounding resistances following replacement of rod electrodes by mesh electrodes on 1 August 2013 (day 1) and (b) comparison of grounding resistances of rod versus mesh electrodes on the same day of the years 2013 and 2014. The height of the boxes represents the interquartile range, and the horizontal bar represents the median value. The ends of the whiskers extend to the maximum and minimum (average) values recorded for the given data set. Ground temperatures are measured at a 20 cm depth.

Grounding resistance time series

Figure 9a–9c shows a time series of focus-one resistances collected at the three monitoring sites in Qeqertarsuaq (plate electrodes), Sisimiut (rod electrodes), and Ilulissat (mesh electrodes).

The measured focus-one resistances were observed to be log-normal distributed at all sites, thus supporting the assumptions made in the statistical analysis of laboratory and field experiments. The observation is illustrated by histograms of the focus-one resistances observed at the Ilulissat monitoring site in summer and winter (see Figure 9d). The winter distribution exhibits a more regular bell shape than the summer distribution. The difference is linked to the change in the physical state of the soil over the seasons. In summer, the soil is unfrozen, and environmental parameters, such as temperature and soil moisture content, may change rapidly due to, e.g., precipitation or drought. Such events significantly affect the measured grounding resistances. In winter, however, the ground is frozen, and a change in moisture content and resistivity is linked mainly to the diurnal variations in temperature and thus plays a less significant role.

At the Ilulissat site, focus-one resistances range in summer from 0.19 to 1.4 kΩ, with a geometric mean (scale, e^{μ}) of 0.48 kΩ and a shape factor (σ) of 0.4. In winter, the measured resistances increase by approximately two orders of magnitude, ranging from 9.3 to 180 kΩ with a mean of 33 kΩ and a shape factor of 0.5.

At Qeqertarsuaq, the time series covers one freeze-up period. The measured focus-one resistances are very stable in summer ranging from 1.6 to 8.1 kΩ with a geometric mean of 2.6 kΩ and a shape factor of 0.2. In winter, the focus-one resistances are also around two orders of magnitude higher, ranging from 110 to 1.2 MΩ with a geometric mean of 344 kΩ and a shape factor of 0.4. The 1.2 MΩ is close to the upper limit of the instrument measurement range, some electrodes were indeed not measurable, and resistivity measurements suffered significantly from the high grounding resistances (see details in Doetsch et al., 2015).

The Sisimiut time series is sparse due to manual data collection, and it covers only a fall/winter season. The winter focus-one measurements range from 18 to 1.2 MΩ with a geometric mean of 203 kΩ and a shape factor of 1.0. At this site, resistivity measurements were also significantly affected by the high grounding resistances, sometimes to a point where measurements were not possible.

In an attempt at evaluating the relative contribution of the geometric effects (perfect grounding) and additional grounding resistance, we have calculated for each site the theoretical perfect single-electrode grounding resistances of equivalent spheroidal electrode models. Spheroids are ellipsoids of revolution, and their surface potential, and thus the grounding resistance, may be calculated using simple analytical expressions given by Ingeman-Nielsen et al. (2016) and T. Ingeman-Nielsen and S. Tomaškovičová (personal communication, 2015), under the assumption that the ground is a homogeneous half-space. We approximated the rod electrodes by a prolate spheroidal model of similar length and radius, and we approximated the plate and mesh electrodes by oblate spheroidal models of similar thickness and areal extent ($\beta = \sqrt{s^2/\pi}$, where s is the plate side length and β is the oblate spheroid major axis); see Figure 10. The grounding resistances of electrodes under perfectly grounded conditions are proportional to the resistivity of the half-space into which they are inserted (Ingeman-Nielsen et al., 2016), and the proportionality factors we have calculated for the electrodes used in this study are listed in Table 4 together with the properties of the spheroidal models applied.

To obtain a time series of equivalent half-space resistivities for each site, we used the normal four-electrode apparent resistivity measurements obtained during automated ERT measurements and calculated weighted averages on a daily basis. The theoretical

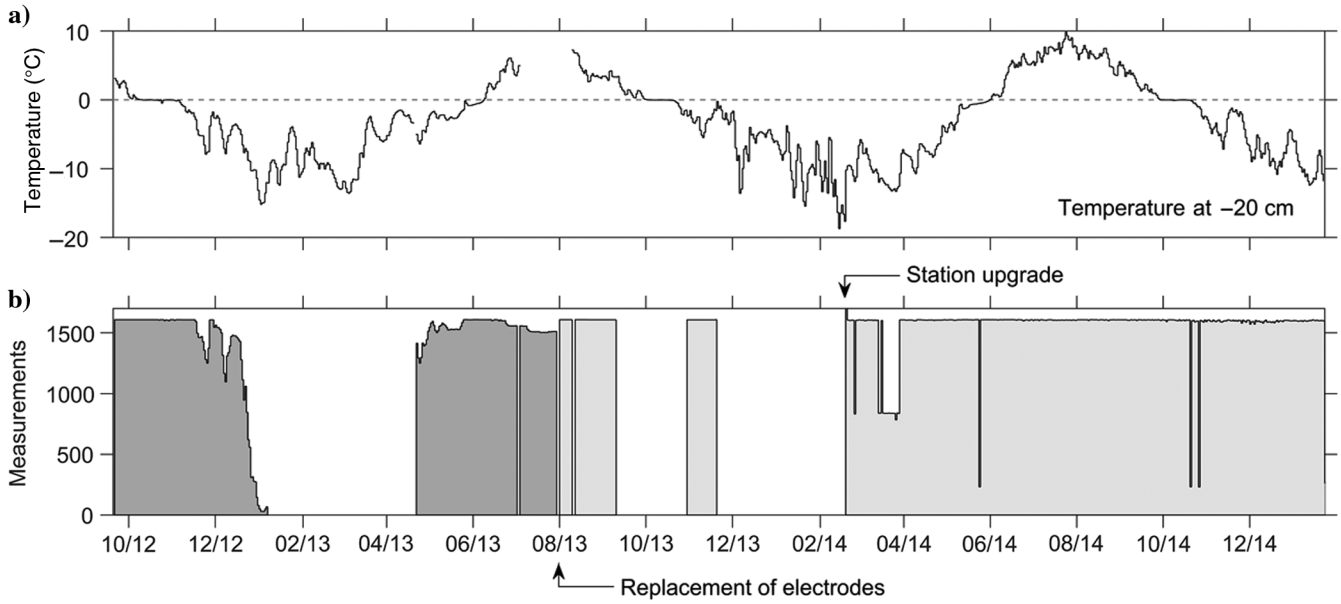

Figure 8. (a) Average daily ground temperature at 20 cm depth at the ERT monitoring site in Ilulissat between 21 September 2012 and 22 January 2015 and (b) the number of collected resistivity measurements on a daily basis. Date ticks indicate the first day of every second month. The dark-gray shading indicates rod electrodes, and the light-gray shading indicates mesh electrodes. A complete day record comprises 1625 measurements. The periods with zero records (such as from 7 January 2013 to 22 April 2013) are due to the Terrameter software malfunction. After the station was upgraded to remote control (19 February 2014), we have not experienced a complete software failure.

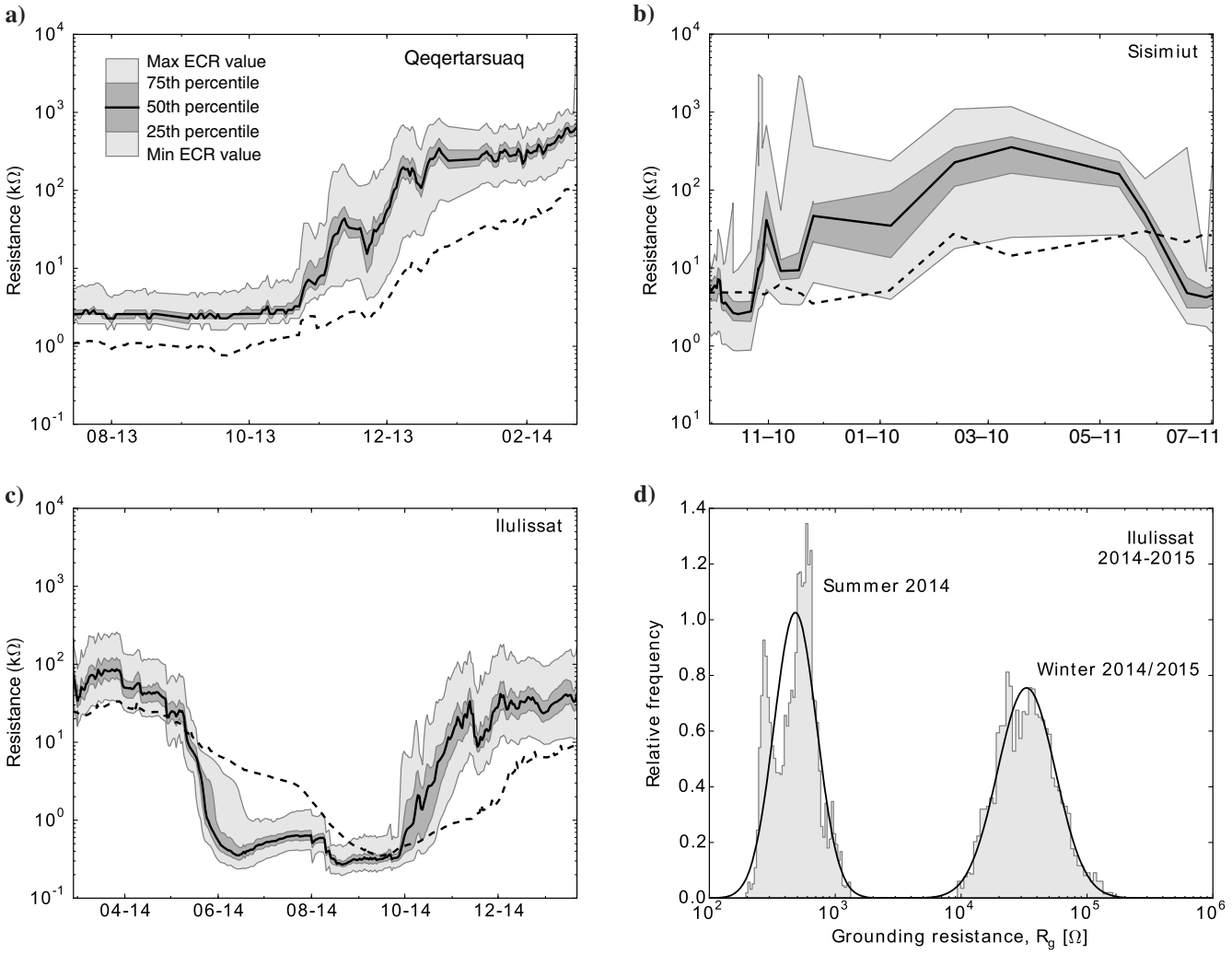

Figure 9. Time series of measured focus-one resistances (grounding resistances) for the monitoring stations in (a) Qeqertarsuaq, (b) Sisimiut, and (c) Ilulissat. The plots show mean array grounding resistance (the solid black line), 25th and 75th percentiles (the dark-gray shading), and maximum and minimum measured values (the light-gray shading). The plots also show the theoretical grounding resistance of a perfectly grounded electrode using estimated half-space resistivities based on the measured average daily apparent resistivities for each profile (dashed black line). The histograms in panel (d) illustrate the log-normal distribution of grounding resistances observed in Ilulissat in summer (1 July 2014 to 1 September 2014) and winter (1 December 2014 to 31 January 2015).

Table 4. Properties of physical electrodes used in monitoring applications and the equivalent spheroidal electrode models used in interpretation.

	Rods	Plates	Meshes
Installed at locality	Sisimiut	Qeqertarsuaq	Ilulissat
Electrode dimensions	$\phi = 1.0$ cm, $L = 10.0$ cm	$10 \times 10 \times 0.6$ cm ($h \times w \times t$)	$10 \times 10 \times 0.6$ cm ($h \times w \times t$)
Burial depth	−0.1 m	−0.1 m	−0.2 m
Model type	Prolate spheroid	Oblate spheroid	Oblate spheroid
Model dimensions	$\alpha = 0.5$ cm, $\beta = 5$ cm	$\alpha = 3$ mm, $\beta = 5.6$ cm	$\alpha = 3$ mm, $\beta = 5.6$ cm
Rotational symmetry around	y-axis	x-axis	x-axis
Grounding resistance	$5.182\ \mathrm{m}^{-1} \cdot \rho$	$2.551\ \mathrm{m}^{-1} \cdot \rho$	$2.344\ \mathrm{m}^{-1} \cdot \rho$

perfect grounding resistances were then calculated by multiplying the daily time series of half-space resistivities for a particular site by the appropriate proportionality constant listed in Table 4. These time series are included in the plots in Figure 9a–9c as dashed lines.

Obviously, using a homogeneous half-space resistivity is not very appropriate in a setting in which top-down freezing and thawing cause a layered earth structure with large resistivity contrasts. The problem is most clearly visible in the Ilulissat data, in which focus-one resistances drop as the ground thaws, but the estimated perfect grounding resistance only drops gradually over the summer because the thawing progresses and affects a larger part of the resistivity measurements used for the half-space approximation. This indicates that the focus-one protocol is highly sensitive to 2D and 3D ground resistivity variations.

At the Qeqertarsuaq site, the estimated perfect grounding resistance is consistently lower than the observed focus-one resistances, typically by a factor of two or more to the best grounded electrodes. At the Ilulissat and Sisimiut sites, however, during some parts of the year, the estimated perfect grounding resistance is approximately coincident with the minimum measured focus-one resistance. Furthermore, the estimated perfect grounding resistance never reaches the very high resistance values measured at some electrodes in wintertime.

Therefore, it seems an appropriate first approximation to consider the best grounded electrode of the layout to be perfectly grounded and consider the span of focus-one resistances on any given day as a conservative estimation of the additional grounding resistance. Thereby, we implicitly assume the half-space properties to be invariable along the layout and the additional grounding resistance R_a to be positively valued.

Under these assumptions, the additional grounding resistances in summer range from 0 to 1.2 kΩ and 6.5 kΩ at the Ilulissat and Qeqertarsuaq sites, respectively. The estimated additional grounding resistance in winter is up to three orders of magnitude larger, ranging from 0 to 170 kΩ at the Ilulissat monitoring station and up to more than 1 MΩ at the Qeqertarsuaq and Sisimiut monitoring stations.

DISCUSSION

There is a clear benefit in focusing on the evaluation of grounding resistance data from Arctic tundra landscapes. The environmental settings give rise to some of the most extreme conditions for ERT; on the one hand, the thawed, moisture-saturated ground provides very favorable conditions for good grounding of electrodes in the summer season. On the other hand, extremely high grounding resistances encountered upon ground freezing make it difficult to carry out surveys and monitoring projects throughout the winter. The challenge is to design a monitoring array that can sustain and perform in both extreme scenarios.

The problem of high grounding resistances is threefold. The most immediate problem concerns the total resistive load of the current transmission circuit. High loads require high supply voltages to drive even small currents, and they may challenge the ability of the acquisition system to stabilize the transmitted currents (Doetsch et al., 2015). The result may be noisy measurements, if measuring is at all possible. If the transmitted current is correctly stabilized, very high grounding resistances of the current electrodes may result in small transmitted currents and correspondingly lower signal levels at the receiver (depending on the ground resistivity structure), causing increased S/N, as pointed out in an early study by Rooney and Gish (1927). The third issue relates to leakage currents through the receiver circuitry at high grounding resistances of the receiver electrodes. LaBrecque et al. (2007) present a simple model using a grounding resistance of 10 kΩ and internal instrument resistance of 10 MΩ. They conclude that the combination results in errors of approximately 0.2% in measured voltages and thus apparent resistivities. Through a more complex model, which takes into account the size, shape, and positioning of the electrodes, T. Ingeman-Nielsen and S. Tomaškovičová (personal communication, 2015) describe systematic measurement errors due to receiver electrode grounding resistances. According to their model, grounding resistances in the upper range of values observed in this study would lead to errors in resistivity measurements on the order of 10% or more at receiver input impedances of around 10 MΩ. Choosing an optimized electrode design for ERT studies in cold regions could therefore not only prolong the period of acquisition but also improve the quality of measurements and accuracy of interpretations.

For this study, we used two different types of instruments. The ABEM Terrameter SAS 1000 has a fixed receiver input impedance of 10 MΩ, whereas the ABEM Terrameter LS has a receiver input impedance ranging from 200 MΩ at the highest gain setting (±2.5 V) to 20 MΩ at the lowest gain setting (±600 V). For normal resistivity measurements, these are the values to consider. However, when doing focus-one measurements, typically the receiver circuitry is connected in parallel with the transmitter circuitry, and thus any impedance associated with the current transmission circuitry needs to be taken into account. The SAS 1000 instrument transmission circuitry has very high (but unspecified) impedance (P. Hedblom, personal communication, 2015). The effective impedance of the instrument is therefore assumed close to 10 MΩ when doing focus-one measurements with current and potential terminals connected in parallel. The Terrameter LS, however, has separate monitoring channels permanently connected to the transmission circuitry and a resulting effective impedance of 6 MΩ or greater (depending on the gain). Thus, based on the findings of Ingeman-Nielsen

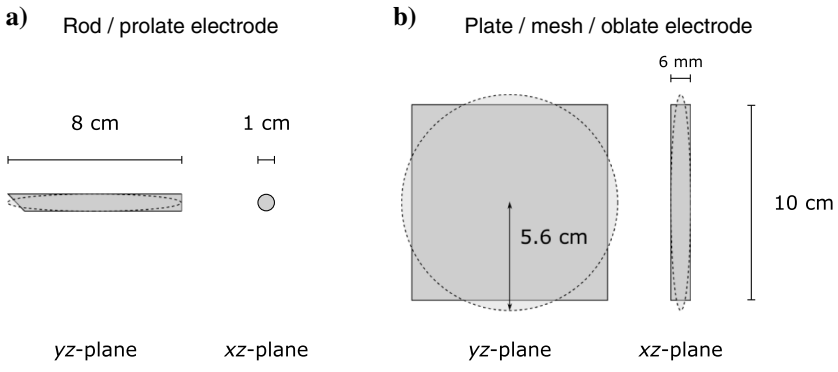

Figure 10. Schematic representation of electrode types and equivalent spheroidal models: (a) the rod electrodes are approximated by prolate spheroids of the same length and (b) the plate and mesh electrodes are approximated by oblate spheroids with similar areal extent and thickness. The coordinate system is oriented such that the electrode array direction is along the x-axis.

et al. (2016), the focus-one measurements collected with the two instruments are typically accurate to within ±7% and ±12% (focus-one resistances typically underestimated), SAS 1000 and LS, respectively, for the monitoring arrays of 64 electrodes or more, and to within ±19% and ±21% (focus-one resistances typically overestimated) for the short 10-electrode arrays. These specified ranges correspond to R_v/ρ ratios of 1000 and 500 m^{-1}, for the SAS 1000 and LS instruments, respectively.

Although automated profile focus-one measurements with the SAS 1000 are performed using the calibrated standard measurement channel, the current Terrameter LS firmware uses an uncalibrated internal transmitter monitoring channel (P. Hedblom, personal communication, 2015). Analysis of the full time series of resistivity measurements from Qeqertarsuaq indicates that the uncalibrated channel voltage measurement is typically within ±10% of the voltage measured by a calibrated monitoring channel. This additional measurement uncertainty relates only to the automated grounding resistance measurement time series from Qeqertarsuaq. The short array electrode field tests are measured manually using the standard measurement channel and are therefore not affected.

Understanding the changes of grounding resistances in cold regions requires insight into processes that condition the resistivity of half-space and a possible alteration zone around the electrode. The bulk ground resistivity depends on four main factors: soil mineralogic composition, porosity, fraction of unfrozen pore water, and geochemical composition of the pore water (e.g., Hoekstra et al., 1975; Friedman, 2005). An aqueous solution is, in most cases, the only conducting phase in the soil. In practice, it is also the only phase that substantially changes proportions over the course of a year. The processes of drying out and freezing (fall/winter) and thawing and infiltration (spring/summer) control not only the moisture content but also concentration of solutes in the unfrozen pore water.

When trying to evaluate the contribution of respective environmental effects in field experiments, it is impossible to properly control the numerous factors influencing ground resistivity. However, the experiment we conducted in the laboratory allowed us to control some of the most important factors, such as soil type, soil moisture content, and temperature. Due to the scale of the experiment, the laboratory results are not quantitatively comparable to field results. The geometric effects of the small buckets alter the current paths and impact of the embedding medium. Indeed, the grounding resistances measured in the field were typically several orders of magnitude higher than values obtained at similar temperatures in the laboratory. Nevertheless, the experiments in the controlled environment allowed us to qualitatively confirm the findings of the field observations and observing the cryostructure occurring around electrodes.

The horizontally oriented plate electrodes were included in the laboratory tests based on a recommendation (T. Dahlin, personal communication, 2013) that such an electrode configuration had been successfully implemented in a monitoring system under temperate conditions to improve moisture retention around the electrodes and thus decrease grounding resistances. The effect under frozen conditions, however, proved opposite due to preferential ice buildup around the electrode, and thus it was decided not to consider that electrode configuration for long-term field experiments in the Arctic. Although increasing the size of electrodes reduces the grounding resistance, it may also inflict geometric errors on resistivity measurements, especially when electrode separations are short (Igel, 2007). This effect has not been investigated in the current study.

CONCLUSIONS

It is widely recognized that high grounding resistances negatively influence ERT acquisitions in terms of the amount and quality of measured data. In monitoring applications in cold climates, the grounding resistance becomes the limiting factor of successful acquisition of meaningfully long time series, and high grounding resistances often restrict the measurements to the short summer season. We found that modifications to the electrode design bring significant ($p < 0.01$) improvements to the performance of an ERT array that operates under ground freezing conditions.

Our 3^3 factorial field experiment (three sites, three electrode types, and three seasons) provides a thorough and coherent analysis of electrode performance under realistic field conditions. It addresses the main effect of electrode size by testing rod electrodes against two similarly sized square electrodes (plates and meshes). It also considers the surface area and alteration zone effects, by comparing electrodes of similar size, but different surface area and construction design (plates and meshes). Finally, lithologic/resistivity effects are treated by repeating the same experiments at multiple sites and multiple seasons.

We conclude that increasing the electrode size (using plates or meshes instead of rods) significantly ($p < 0.01$) reduces the grounding resistance (by 28%–69%) at all sites and all seasons (thawed and frozen ground conditions). Furthermore, changing the electrode construction from plates to meshes further improves the grounding resistance in winter (frozen ground conditions) by 29%–37% at two out of three sites. At the Sisimiut site, plate and mesh electrodes performed equally well.

As the plate and mesh electrodes are similarly shaped, the main difference is in the effective surface area of the electrodes, which is five times larger for the mesh electrodes. The increased effective surface area seems to be an advantage when the electrodes are inserted or buried in fine-grained mineral or organic soils with some cohesive properties, in which the soil may fill the mesh openings. In coarser grained soils under well-drained conditions, it is unlikely that full advantage is taken of the larger surface area, which is probably the reason mesh electrodes did not constitute an improvement over plate electrodes at the Sisimiut site. The mesh electrodes may even provide less surface area than the plates if placed on hard surfaces such as rock outcrops, unless a wetting or contact agent such as moist clay, mud, or a sponge is used as part of the installation.

We speculate that the thermal properties of electrodes also play a role in the performance of the electrodes in cryospheric applications. Preferential freezing around the electrodes due to the changing heat flow in the soil caused by heat conduction through the electrode may counteract the benefit of increasing the size of massive electrodes. This would be a significant process in fine-grained soils in which capillary forces could result in vertical and horizontal moisture transport and ice buildup during ground freezing, as indicated by the cryostructure observed around plate electrodes in the laboratory experiment.

In spite of these reservations, the advantage of applying an optimized electrode design is documented at the Ilulissat permanent ERT monitoring station. The replacement of 64 rod electrodes by mesh electrodes resulted in an immediate reduction in the average grounding resistance by 73%, from 1.5 to 0.4 kΩ. Compa-

rable winter grounding resistances improved by 61%, from an average of 64.1 to 25.2 kΩ.

Time series of focus-one grounding resistances from long-term monitoring arrays at the three field sites document that grounding resistances are lognormally distributed and correlated to temperature (ground freezing). Summer grounding resistances at Ilulissat and Qeqertarsuaq monitoring stations range from 0.2 to 8.1 kΩ and may increase by more than two orders of magnitude upon ground freezing. Values of more than 1 MΩ were observed at the Qeqertarsuaq and Sisimiut monitoring stations. These observations support the conclusion that choosing an optimized electrode design, in this case the mesh electrodes, may make the difference between being able to collect measurements or not during the most challenging parts of the year.

With this paper, we present the first complete and coherent study of electrode grounding resistances under adverse environmental conditions, and we document the range of contact resistance values that can be expected in field situations in cold climates. We also quantitatively demonstrate the general understanding that increasing the electrode size and surface area decreases the electrode grounding resistance.

We expect the insight provided in this study to pave the way for future improvement in acquisition systems designed for proper monitoring of grounding resistances and improved accuracy in standard resistivity and IP measurements. This is of particular importance in monitoring applications in which minute changes in the resistivity structure are of interest. To enhance resolution and applicability of the ERT method and to improve our chances of correct data interpretation, we also see a need to incorporate the grounding resistance information into the data processing and inversion algorithms.

ACKNOWLEDGMENTS

Funding for this study was provided to B. Elberling by the Danish National Research Foundation (CENPERM DNRF100) and is part of a larger research program at 10 sites in Greenland. The authors would like to thank the Arctic Station for supplying a logistical platform and the permits for the work in Qeqertarsuaq and N. Foged for his help with calibrating instruments. We also wish to thank R. Nielsen, S. Mulvad, K. Trabjerg, S. Høgsholt, and M.T. Christensen for their contribution to the field and laboratory work.

REFERENCES

Arenson, L., D. Xia, D. Sego, and K. Biggar, 2005, Brine and unfrozen water migration during the freezing of Devon silt: Proceedings of the 4th Biennial Workshop on Assessment and Remediation of Contaminated Sites in Arctic and Cold Climates, 35–44.

Athanasiou, E. N., P. I. Tsourlos, G. N. Vargemezis, C. B. Papazachos, and G. N. Tsokas, 2007, Non-destructive DC resistivity surveying using flat-base electrodes: Near Surface Geophysics, **5**, 263–272, doi: 10.3997/1873-0604.2007008.

Baines, D., D. G. Smith, D. G. Froese, P. Bauman, and G. Nimeck, 2002, Electrical resistivity ground imaging (ERGI): A new tool for mapping the lithology and geometry of channel-belts and valley-fills: Sedimentology, **49**, 441–449, doi: 10.1046/j.1365-3091.2002.00453.x.

Branco, R. M. G. C., A. N. Amorim, J. A. Martins, S. B. Lima, N. C. Pedrosa, N. C. C. Vieira, and K. M. L. Oliveira, 2013, 2D/3D electrical resistivity tomography (ERT) applied to preliminary economic/geoelectrical evaluation of Jandaira and Açu Formations in the SW border of Potiguar Basin, Rio Grande do Norte, Brazil: 13th International Congress of the Brazilian Geophysical Society and EXPOGEF, Extended Abstracts, 574–577.

Brown, J., O. J. Ferrians, Jr., J. A. Heginbottom, and E. S. Melnikov, 1998, Circum-Arctic map of permafrost and ground ice conditions: National Snow and Ice Data Center, digital media, http://nsidc.org/data/docs/fgdc/ggd318_map_circumarctic/, accessed February 2015.

Dabas, M., A. Hesse, and J. Tabbagh, 2000, Experimental resistivity survey at Wroxeter archaeological site with a fast and light recording device: Archaeological Prospection, **7**, 107–118, doi: 10.1002/1099-0763(200006)7:2<107::AID-ARP138>3.0.CO;2-0.

Doetsch, J., T. Ingeman-Nielsen, A. V. Christiansen, G. Fiandaca, E. Auken, and B. Elberling, 2015, Direct current (DC) resistivity and induced polarization (IP) monitoring of active layer dynamics at high temporal resolution: Cold Regions Science and Technology, **119**, 16–28, doi: 10.1016/j.coldregions.2015.07.002.

Friedman, S., 2005, Soil properties influencing apparent electrical conductivity: A review: Computers and Electronics in Agriculture, **46**, 45–70, doi: 10.1016/j.compag.2004.11.001.

Hansen, B. U., B. Elberling, O. Humlum, and N. Nielsen, 2006, Meteorological trends (1991–2004) at Arctic Station, Central West Greenland (69° 15′N) in a 130 years perspective: Danish Journal of Geography, **106**, 45–55, doi: 10.1080/00167223.2006.10649544.

Hauck, C., and D. Vonder Mühll, 2003, Permafrost monitoring using time-lapse resistivity tomography, *in* M. Phillips, S. M. Springman, and L. U. Arenson, eds., Permafrost: Swets & Zeitlinger, 361–366.

Hilbich, C., C. Fuss, and C. Hauck, 2011, Automated time-lapse ERT for improved process analysis and monitoring of frozen ground: Permafrost and Periglacial Processes, **22**, 306–319, doi: 10.1002/ppp.732.

Hoekstra, P., P. Sellmann, and A. Delaney, 1975, Ground and airborne resistivity surveys of permafrost near Fairbanks, Alaska: Geophysics, **40**, 641–656, doi: 10.1190/1.1440555.

Hördt, A., P. Weidelt, and A. Przyklenk, 2013, Contact impedance of grounded and capacitive electrodes: Geophysical Journal International, **193**, 187–196, doi: 10.1093/gji/ggs091.

Igel, J., 2007, On the small-scale variability of electrical soil properties and its influence on geophysical measurements: Ph.D. dissertation, University of Frankfurt/Main.

Ingeman-Nielsen, T., 2005, Geophysical techniques applied to permafrost investigations in Greenland: Ph.D. dissertation, Technical University of Denmark.

Ingeman-Nielsen, T., S. Tomaškovičová, and T. Dahlin, 2016, Effect of electrode shape on grounding resistances — Part 1: The focus-one protocol: Geophysics, **80**, this issue, doi: 10.1190/geo2015-0484.1.

Kneisel, C., 2006, Assessment of subsurface lithology in mountain environments using 2D resistivity imaging: Geomorphology, **80**, 32–44, doi: 10.1016/j.geomorph.2005.09.012.

Kneisel, C., and C. Hauck, 2008, Electrical methods, *in* C. Hauck, and C. Kneisel, eds., Applied geophysics in periglacial environments: Cambridge University Press, 3–27.

LaBrecque, D., and D. Daily, 2008, Assessment of measurement errors for galvanic-resistivity electrodes of different composition: Geophysics, **73**, no. 2, F55–F64, doi: 10.1190/1.2823457.

LaBrecque, D., W. Daily, and P. Atkins, 2007, Systematic errors in resistivity measurement systems: Proceedings of the 20th Symposium on the Application of Geophysics to Engineering and Environmental Problems, EEGS, 1153–1160.

Lundström, K., R. Larsson, and T. Dahlin, 2009, Mapping of quick clay formations using geotechnical and geophysical methods: Landslides, **6**, 1–15, doi: 10.1007/s10346-009-0144-9.

Montgomery, D. C., 1997, Design and analysis of experiments: John Wiley & Sons.

Reynolds, J. M., 1997, An introduction to applied and environmental geophysics: Wiley.

Rooney, W. J., and O. H. Gish, 1927, Results of earth-resistivity surveys near Watheroo, Western Australia, and at Ebro, Spain: Terrestrial Magnetism and Atmospheric Electricity, **32**, 49–63, doi: 10.1029/TE032i002p00049.

Rosset, E., C. Hilbich, S. Schneider, and C. Hauck, 2013, Automatic filtering of ERT monitoring data in mountain permafrost: Near Surface Geophysics, **11**, 423–433, doi: 10.3997/1873-0604.2013003.

Scott, W., P. Sellmann, and J. Hunter, 1990, Geophysics in the study of permafrost, *in* S. Ward, ed., Geotechnical and environmental geophysics: SEG, 355–384.

Sunde, E. D., 1949, Earth conduction effects in transmission systems: Dover Van Nostrand Company Inc..

Telford, W. M., L. P. Geldart, and R. E. Sheriff, 1990, Applied geophysics: Cambridge University Press.

Tukey, J. W., 1949, Comparing individual means in the analysis of variance: Biometrics, **5**, no. 2, 99–114, doi: 10.2307/3001913.

Vonder Mühll, D., C. Hauck, H. Gubler, R. McDonald, and N. Russill, 2001, New geophysical methods of investigating the nature and distribution of mountain permafrost with special reference to radiometry techniques: Permafrost and Periglacial Processes, **12**, 27–38, doi: 10.1002/ppp.382.

Wait, J. R., 1982, Geo-electromagnetism: Academic Press.

Zonge, K., J. Wynn, and S. Urquhart, 2005, Resistivity, induced polarization and complex resistivity, *in* D. K. Butler, ed., Near-surface geophysics: SEG, 265–300.